



HAL
open science

Multiplexed Quantitation of Intraphagocyte Mycobacterium tuberculosis Secreted Protein Effectors

Fadel Sayes, Catherine Blanc, Louis S Ates, Nathalie Deboosere, Mickael Orgeur, Fabien Le Chevalier, Matthias I Gröschel, Wafa Frigui, Ok-Ryul Song, Richard Lo-Man, et al.

► **To cite this version:**

Fadel Sayes, Catherine Blanc, Louis S Ates, Nathalie Deboosere, Mickael Orgeur, et al.. Multiplexed Quantitation of Intraphagocyte Mycobacterium tuberculosis Secreted Protein Effectors. Cell Reports, 2018, 23 (4), pp.1072-1084. 10.1016/j.celrep.2018.03.125 . pasteur-02046037

HAL Id: pasteur-02046037

<https://pasteur.hal.science/pasteur-02046037v1>

Submitted on 22 Feb 2019

HAL is a multi-disciplinary open access archive for the deposit and dissemination of scientific research documents, whether they are published or not. The documents may come from teaching and research institutions in France or abroad, or from public or private research centers.

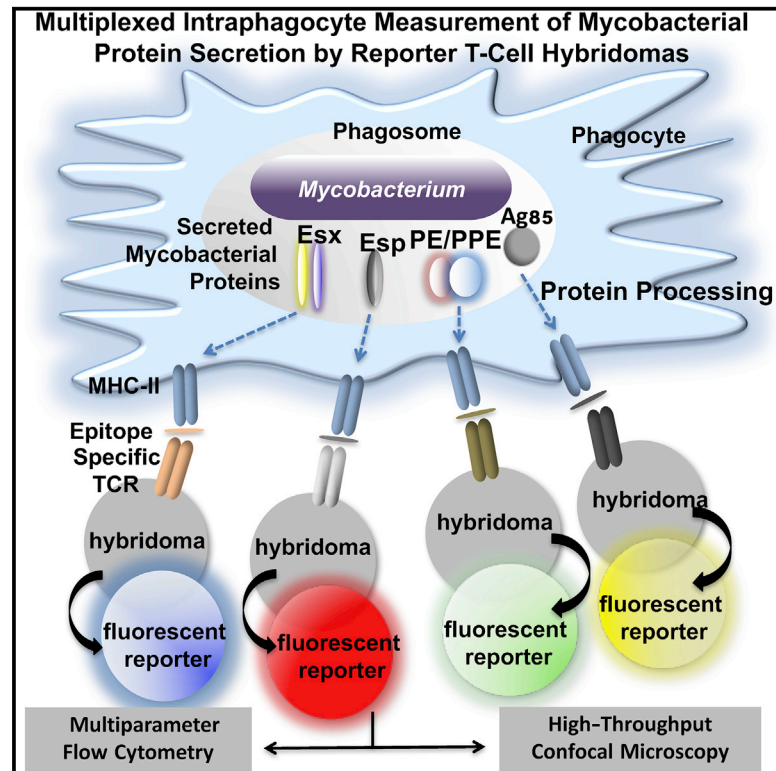
L'archive ouverte pluridisciplinaire **HAL**, est destinée au dépôt et à la diffusion de documents scientifiques de niveau recherche, publiés ou non, émanant des établissements d'enseignement et de recherche français ou étrangers, des laboratoires publics ou privés.



Distributed under a Creative Commons Attribution - NonCommercial - NoDerivatives 4.0 International License

Multiplexed Quantitation of Intraphagocyte *Mycobacterium tuberculosis* Secreted Protein Effectors

Graphical Abstract



Authors

Fadel Sayes, Catherine Blanc, Louis S. Ates, ..., Pierre Charneau, Roland Brosch, Laleh Majlessi

Correspondence

laleh.majlessi@pasteur.fr

In Brief

Sayes et al. develop an approach to express distinct fluorescent reporters that is based on the recognition of specific *Mycobacterium tuberculosis* MHC class II epitopes by highly discriminative T cell hybridomas. This multiplexed technology allows the study of secretion, subcellular location, and regulation patterns of these instrumental protein members.

Highlights

- T cell hybridomas detect individual mycobacterial proteins without cross-reactivity
- Detection of mycobacterial proteins by T cells allows visualization of their cellular topography
- Measurement of intraphagocyte mycobacterial proteins can be performed with T cells
- A multiplexed assay of mycobacterial protein quantitation has numerous applications



Multiplexed Quantitation of Intraphagocyte *Mycobacterium tuberculosis* Secreted Protein Effectors

Fadel Sayes,¹ Catherine Blanc,² Louis S. Ates,¹ Nathalie Deboosere,³ Mickael Orgeur,¹ Fabien Le Chevalier,¹ Matthias I. Gröschel,¹ Wafa Frigui,¹ Ok-Ryul Song,³ Richard Lo-Man,⁴ Florence Brossier,^{1,5} Wladimir Sougakoff,⁵ Daria Bottai,⁶ Priscille Brodin,³ Pierre Chameau,² Roland Brosch,¹ and Laleh Majlessi^{1,7,*}

¹Institut Pasteur, Unit for Integrated Mycobacterial Pathogenomics, CNRS UMR 3525, 25 rue du Dr. Roux, Paris 75015, France

²Institut Pasteur, Unit for Molecular Virology and Vaccinology, 28 rue du Dr. Roux, Paris 75015, France

³Université de Lille, CNRS UMR 8204, INSERM U1019, CHU Lille, Institut Pasteur de Lille, Center for Infection and Immunity of Lille (CIIL), 1 rue du Professeur Calmette, 59000 Lille, France

⁴Institut Pasteur, Neonatal Immunity Group, Unit for Human Histopathology and Animal Models, 28 rue du Dr. Roux, Paris 75015, France

⁵Sorbonne Universités, UPMC University of Paris 06, CIMI-Paris, AP-HP, Hôpital Pitié-Salpêtrière, CNR-MyRMA, Paris, France

⁶University of Pisa, Department of Biology, via S. Zeno 35-39, 56127 Pisa, Italy

⁷Lead Contact

*Correspondence: laleh.majlessi@pasteur.fr

<https://doi.org/10.1016/j.celrep.2018.03.125>

SUMMARY

The pathogenic potential of *Mycobacterium tuberculosis* largely depends on ESX secretion systems exporting members of the multigenic Esx, Esp, and PE/PPE protein families. To study the secretion and regulation patterns of these proteins while circumventing immune cross-reactions due to their extensive sequence homologies, we developed an approach that relies on the recognition of their MHC class II epitopes by highly discriminative T cell receptors (TCRs) of a panel of T cell hybridomas. The latter were engineered so that each expresses a unique fluorescent reporter linked to specific antigen recognition. The resulting polychromatic and multiplexed imaging assay enabled us to measure the secretion of mycobacterial effectors inside infected host cells. We applied this novel technology to a large panel of mutants, clinical isolates, and host-cell types to explore the host-mycobacteria interplay and its impact on the intracellular bacterial secretome, which also revealed the unexpected capacity of phagocytes from lung granuloma to present mycobacterial antigens via MHC class II.

INTRODUCTION

Full virulence of the tuberculosis agent *Mycobacterium tuberculosis* (*Mtb*) depends on functional ESX/type VII secretion systems (T7S), such as ESX-1, ESX-3, and ESX-5 (Gröschel et al., 2016). ESX-1-secreted substrates include EsxA (ESAT-6), EsxB (CFP-10), and several ESX-1 secretion-associated proteins (Esp) encoded inside the *esx-1* locus or outside the *esx-1* region, such as the *espA-espC-espD* operon (Figure S1A). These proteins are key players in the interaction of the pathogen with

the host immune cells (Gröschel et al., 2016; Stanley and Cox, 2013). The ESX-3 system plays a critical role in iron acquisition and export of EsxG and EsxH, which are also involved in virulence and immunogenicity (Majlessi et al., 2015). ESX-5 is the most recently evolved ESX system, and it plays a role in outer membrane permeability (Ates et al., 2015; Di Luca et al., 2012; Dumas et al., 2016). ESX-5 exports not only multiple Esx proteins but also a plethora of proteins harboring N-terminal PE or PPE motifs encoded both inside or outside the *esx-5* region (Figure S1B) (Gey van Pittius et al., 2006). The recently solved structure of ESX-5 can serve as a general model for T7S systems, which involve four Esx-conserved components named EccB, EccC, EccD, and EccE that assemble with equimolar stoichiometry into an oligomeric complex in 6-fold symmetry (Beckham et al., 2017; Houben et al., 2012). Numerous PE/PPE substrates secreted by ESX-5 can modulate the host immunity and represent abundant sources of B cell or T cell epitopes (Bottai et al., 2012; Fishbein et al., 2015; Sayes et al., 2012). However, individual investigation of these proteins is hampered by difficulties in biochemically detecting them because of their high levels of sequence homology (Betts et al., 2000; Ramakrishnan et al., 2015). Considering the prominent roles of T7S systems, tools that can provide reliable detection and quantitation of their secreted substrates would have countless biological applications, including (1) investigation of the functional mechanisms of ESX machineries, (2) study of the fundamental aspects of the T7S substrate antigenic presentation, (3) discovery of anti-tuberculosis (TB) T7S-targeting drugs, and (4) immunogenicity screening of live attenuated vaccine candidates.

The substantial AA sequence similarities among the members of multigenic protein families often preclude their discriminative detection by antibodies. The latter recognize discontinuous conformational epitopes, or 10–22 AA-long continuous motifs, and thus commonly present cross-reactivities toward numerous related epitopes (Van Regenmortel, 2009). Moreover, it is essential to develop intracellular detection assays that can report on the cross-talk between the host cells and its influence on the



ESX secretome of intracellular bacilli (Champion, 2013; Chen et al., 2013). For instance, the ESX-1 system is upregulated in the host maturing phagosomes (Abramovitch et al., 2011; Ates et al., 2016). Reminiscent of type III secretion system regulation (Deane et al., 2010; Dewoody et al., 2013; Ferris and Minamino, 2006), EspB interacts with the host plasma membrane to signal to ESX-1 to control its repertoire of secreted substrates. Secretion of LipY lipase, a PE protein secreted via ESX-5, is induced during infection, but not in axenic culture (Daleke et al., 2011).

Here, we developed a technology that overcomes cross-reactivities, thereby allowing the exclusive detection and semiquantitation of individual T7S substrates inside the phagocytes. This approach is based on the recognition of major histocompatibility complex (MHC) class II-restricted epitopes of T7S substrates by T cell receptors (TCRs). Using a panel of T cell hybridomas that reliably discern different T7S antigens contained in sub-mycobacterial fractions, we gained insights into the topology of such proteins. We further transduced these T cell hybridomas with integrative lentiviral (LV) vectors harboring fluorescent reporter genes whose transcription depends on cognate TCR triggering. After the interaction of TCRs with specific epitopes presented by MHC class II of infected dendritic cells (DCs), the T cells emit specific fluorescent signals. By attributing given reporter signals to each TCR, we set up a multispecific and polychromatic method that we applied to a large panel of mycobacterial *esx* mutants to obtain new information on the contribution of individual ESX core components to intraphagocyte protein secretion. By this approach, we also explored the ability of phagocytes from pulmonary granulomas to present mycobacterial antigens, a pathway whose inhibition is thought to constitute a major mechanism of *Mtb* to evade the host adaptive immunity (Rogerson et al., 2006; Shi et al., 2004).

RESULTS

T Cell Hybridomas Overcome Cross-Reactivity and Exclusively Detect Individual Members of the ESX Multigenic Families

To detect secretion of *Mtb* proteins via the dedicated secretion systems, a panel of mouse T cell hybridomas specific to MHC class II epitopes of various *Esx*, *Esp*, or *PE* substrates was used (Table S2). All involved epitopes were described previously (Hervas-Stubbs et al., 2006; Kamath et al., 2004; Majlessi et al., 2006), except EspC:40–54, which was identified here by EspC epitope mapping (Figures S2A and S2B). BlastP (Altschul et al., 1997) comparison was used to ascertain the absence of sequence homology between the selected epitopes and other *Mtb* proteins. The T cell hybridomas produced the early T cell activation marker interleukin-2 (IL-2), in an epitope contact-dependent manner. IL-2 was detected in co-cultures of T cell hybridomas with isogenic DCs loaded with specific peptides (Figures 1A–1D) or infected with appropriate wild-type (WT) mycobacteria, whereas DCs infected with *esx* deletion mutants did not induce a signal (Figures 1E–1H).

The outstanding discriminative potential of this system was exemplified by the case of T cell hybridomas specific to the ESX-3 substrates. The C-ter *EsxH*:74–88 epitope, with 11/15 sequence identity with its close relative the *EsxR*:74–88 segment

(Table S1), was detected by (1) the 5A8 T cell clone with the same affinity as *EsxR*, (2) the 1H2 clone with 200× higher affinity compared to *EsxR*, and (3) the 1G1 clone in a fully exclusive manner (Figure 1B).

ESX-5-associated PE18 and PE19 proteins are almost identical due to a recent gene duplication event, and they share high sequence similarity with many non-ESX-5 associated PE members. PE18/19 possess the PE18/19:1–18 and PE18/19:35–51 epitopes. The latter is shared with numerous PE homologs encoded outside the *esx-5* region, while the former is highly specific to PE18/19 (Sayes et al., 2012). Appropriate screening versus PE18/19:1–18 allowed the selection of IF6 and IB12 T cell hybridomas able to recognize PE18/19, but not the other PE members. This was observed with DCs infected with WT *Mtb*, but not with the $\Delta ppe25-pe19$ mutant (Figure 1G). The latter is deleted for the segment containing the *pe18*, *pe19*, and 3 *ppe* genes within the *esx-5* locus while preserving an intact *EccD*₅-dependent functional ESX-5 system, through which a plethora of other PE/PPE are secreted (Bottai et al., 2012; Fishbein et al., 2015; Sayes et al., 2012, 2016). DE10 and 2A1 T cell hybridomas (Figures 1D and 1H) were used to detect the Twin-arginine translocation (Tat)-dependent substrates Ag85A/B (Marrichi et al., 2008). Thus, TCRs can be selected to overcome cross-reactivities among the highly homologous mycobacterial secreted proteins.

T Cell-Based Discriminative Detection of T7S Substrates Allows Their Sub-mycobacterial Topography

Biochemical topography approaches depend on the availability of specific antibodies or introduction of protein tags, which may interfere with localization. Here, to map T7S proteins in mycobacteria, DCs incubated with various concentrations of sub-mycobacterial fractions, obtained by ultracentrifugation, were co-cultured with specific T cell hybridomas. If the protein of interest was present in the mycobacterial fraction, it was processed and presented by the DC to the T cell hybridomas. The amounts of IL-2 released by T cells were proportional to T7S protein content in the bacterial fraction. *EsxA* and *EsxB* were detected only in the culture filtrate, whole-cell lysate, and cytosol of WT *Mtb*, not in the total membrane, plasma membrane, or cell wall fractions (Figures 2A and 2B). No *EsxA* or *EsxB* signals were detected in the fractions from the $\Delta esx-1$ mutant, showing the specificity of the assay, in line with data obtained by *EsxA*- or *EsxB*-specific western blotting (Figure 2D). Compared to WT *Mtb*, the cytosol fraction of a $\Delta eccD_1$ mutant contained substantially more *EsxA* and *EsxB* (Figures 2A and 2B), suggesting their cytosolic accumulation in the absence of ESX-1 functionality.

The ESX-5-associated PE18/19 virulence-related factors are also protective antigens. PE19 is linked to changes in cell envelope permeability, suggesting it might perform its role in the cell wall (Bottai et al., 2012). However, biochemical topography studies including epitope-tagged constructs were unsuccessful (Ramakrishnan et al., 2015). With our approach, PE18/19 were detected not only in the culture filtrate, whole-cell lysate, and cytosol of WT or unrelated $\Delta eccD_1$ strains but also in total membrane, plasma membrane, and cell wall fractions (Figure 2C). No PE18/19 signal was detected in the fractions of $\Delta ppe25-pe19$

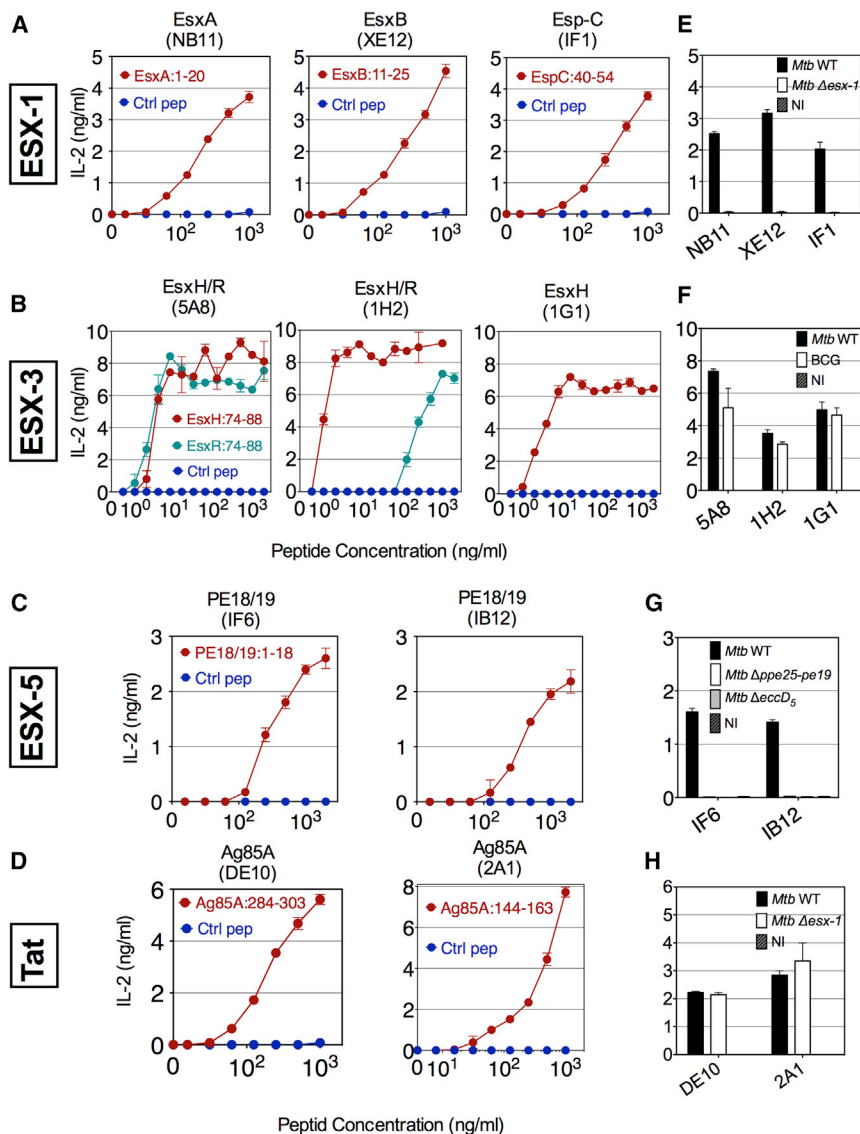


Figure 1. Characteristics of the T Cell Hybridomas Specific to Several T7S Substrates

(A–D) Specificity and sensitivity of T cell hybridomas specific to various substrates of ESX-1 (A), ESX-3 (B), ESX-5 (C), or Tat (D) systems, as determined by their co-culture with DCs, loaded with various concentrations of peptides harboring MHC class II epitopes or negative controls.

(E–H) Capacity of these T cell hybridomas, specific to substrates secreted by ESX-1 (E), ESX-3 (F), ESX-5 (G), or Tat (H) secretion systems, to recognize DCs infected with WT *Mtb* H37Rv, BCG, or appropriate *Mtb* mutants. Shown are concentrations of IL-2 in the co-culture supernatants at 24 hr after T cell addition. Error bars represent the SD of biological co-culture duplicates. Results are representative of 2 experiments. See also Figures S1 and S2 and Table S1.

Even though we do not provide novelty in mycobacterial fractionation, these data illustrate that this non-cross-reactive T cell-based approach can be used to quantify with high sensitivity the exported mycobacterial proteins and to establish the topography of protein effectors in sub-bacterial compartments.

Multiplexed Measurement of Intraphagocyte ESX-1 Substrates

To detect and semiquantitate the secretion of ESX substrates inside the phagocytes, T cell hybridomas were transduced to emit fluorescent reporter signals in response to MHC class II presentation of epitopes from T7S substrates. Integrative LV vectors harboring genes that encode various fluorescent reporters, derived by the murine IL-2 promoter (*Pmil-2*), were constructed (Figure S4) and used to

transduce the T cells. The ZsGreen reporter signal was emitted by the transduced anti-Ag85A/B DE10 T cells, co-cultured with DCs loaded with the specific peptide or infected with diverse *Mtb* or *Bacillus Calmette-Guerin* (BCG) strains, as detectable in an automated confocal microscopy Opera system (Figures 3A and 3B). In parallel, up to 14%–19% of ZsGreen⁺ anti-EsxA NB11 T cells were detected in co-cultures of DCs loaded with homologous peptide or infected only with ESX-1-proficient mycobacteria, indicating the specificity of the assay (Figures 3B and 3C). The percentage of activated ZsGreen⁺ T cells reflected the amount of mycobacterial proteins available within the infected DC.

mutant, indicating the absence of cross-reactivity with the PE homologs encoded outside *esx-5*. For the *ΔeccD5* mutant, a PE18/19 signal was detected in the cytosol and plasma membrane, but not in the cell wall and culture filtrate fractions (Figure 2C). The virulence-related PE18/19 proteins are thus associated to the plasma membrane in an ESX-5-independent manner, possibly by hydrophobic interaction at the cytoplasmic face of the plasma membrane. However, for the translocation to the cell wall and the supernatant, ESX-5-mediated transport is necessary. These data are consistent with the previously reported subcellular localization of the ESX-5 substrate PPE41, associated to the inner plasma membrane in both *Mtb* WT and *ΔeccD5* strains yet associated to the cell wall in the WT strain (Bottai et al., 2012). In *Mycobacterium marinum*, corresponding PE18/19 proteins were also detected in the membrane fraction, culture filtrate, and cytosol fractions (Figure 2E), while EsxB was detected only in the cytosol and culture filtrate.

All T cell hybridomas were subsequently transduced by individual reporters to link each TCR to a given color (Table S3). Recognition of peptide-loaded or *Mtb*-infected DCs resulted in the expression of reporter signals by T cells specific to Tat or T7S substrates (Figure 4A), as detected by cytometry.

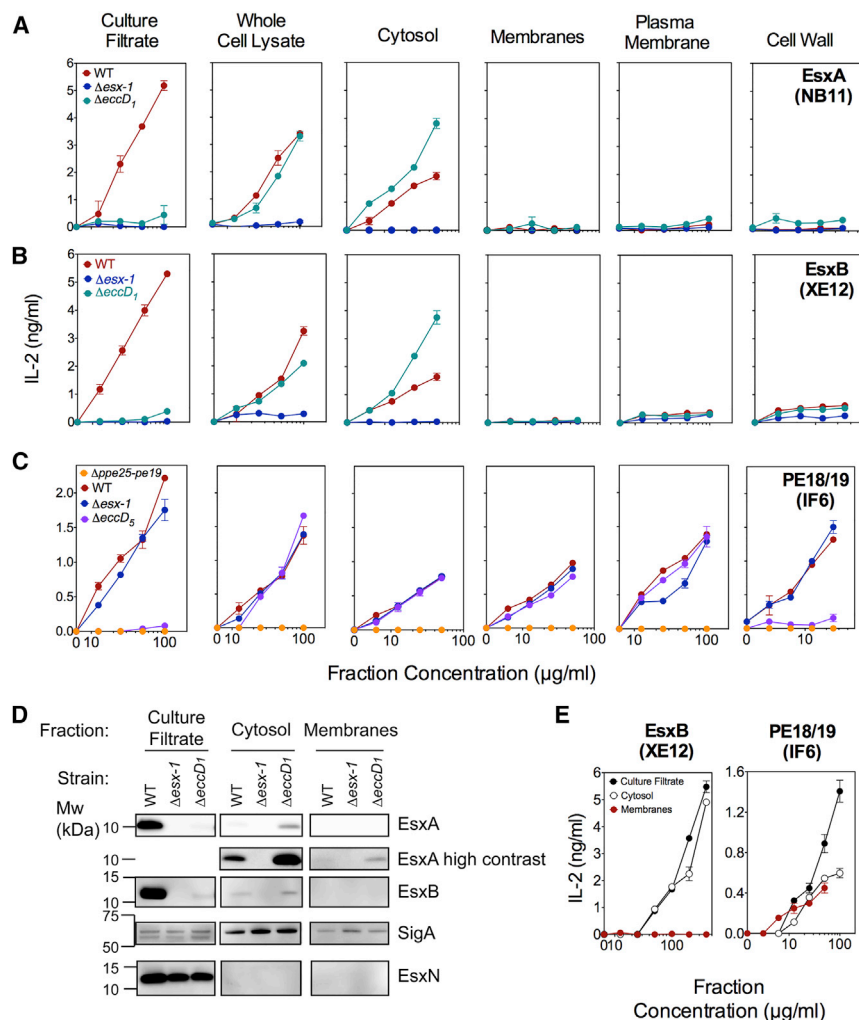


Figure 2. T Cell-Based Topography of T7S Substrates in Mycobacteria Subcellular Compartments

(A–C) Various concentrations of culture filtrates, filtered whole-cell lysates, or different fractions resulting from ultracentrifugation of the whole-cell lysates, prepared from *Mtb* H37Rv WT or appropriate mutants, were added to the co-cultures of DC and EsxA-specific (A), EsxB-specific (B), or PE18/19-specific (C) T cell hybridomas. Shown are concentrations of IL-2 in the co-culture supernatants at 24 hr, which were proportional to the content of T7S-substrate-derived epitopes in the sub-bacterial fractions. The lower detection limit of EsxA- or EsxB-specific T cell hybridomas is 50 ng/mL, and that of PE18/19-specific T cell hybridomas is 150 ng/mL.

(D) Western blot detection of EsxA and EsxB in the same fractions as in (A) and (B). EsxN and SigA detection were performed as positive control for secretion and as lysis and loading control, respectively. Although some SigA was detected in concentrated culture filtrates, this did not vary between strains and could not alternatively explain results. The exclusive detection of PE18/19 by western blot was not possible because of the lack of antibodies able to discern these proteins from their numerous homologs. Results are representative of 2 independent experiments.

(E) Various fractions from *M. marinum* E11 WT assessed for the presence of EsxB or PE18/19, as described for (A)–(C).

Error bars are the SDs of biological co-culture duplicates. See also Figure S3 for the EspC mycobacteria subcellular localization.

Percentage and mean fluorescence intensity (MFI) of reporter⁺ T cells (Figures 4A and S5A), optimal at 24 hr after T cell addition (Figure 5B), were assessed to estimate the relative amounts of proteins released by the intracellular mycobacteria that resulted in processing and presentation by the host DC. A multiplexed analysis of substrate secretion by transduced T cell hybridomas (MASSTT) was developed to simultaneously semiquantitate EsxA, EsxB, and EspC secreted within the phagocytes in a single co-culture well. The distinct reporter signal of each T cell hybridoma was detected in the multiplexed co-cultures by cytometry using a visualization tool for high-dimensional single-cell data based on the t-distributed Stochastic Neighbor Embedding (t-SNE) algorithm (viSNE) (Amir et al., 2013) (Figure 4B) or conventional cytometric analysis (Figures S6A and S6B).

To further extend understanding of intraphagocyte mycobacterial secretion, we MASSTT profiled a panel of *Mtb* mutants and a range of *M. bovis* BCG and *Mycobacterium microti* strains, complemented with WT or single-gene deletion variants of the orthologous *esx-1*^{Mtb} region (BCG::*esx-1* or *M. microti*::*esx-1*) (Table S4) (Brodin et al., 2005, 2006; Pym et al., 2002, 2003).

Principal-component analysis (PCA) of MASSTT data depicted a separation among *Mtb* variants producing, not producing, or barely producing ESX-1 substrates (Figure 5A), which was confirmed by individual analyses of these variants (Figure 5B). The data showed that in intraphagocyte secretion, EsxA, EsxB, and EspC were inter-dependent, correlated, and quantitatively proportional to one another (Figure 5B). Moreover, the absence of EspF and EspG₁ did not affect the intraphagocyte secretion of the detected ESX-1 substrates (Figures 5A and 5B). The absence of PE35 abolished the intraphagocyte secretion of EsxA, EsxB, and EspC, while the truncation of its partner PPE68 only reduced them quantitatively (Figure 5B). We detected no EsxA, EsxB, or EspC signals when using an Δ eccCb₇ mutant. Thus, at least for the ESX-1 substrates, the secretory behavior of intracellular mycobacteria appears to be consistent with that previously reported in physiologically less relevant axenic conditions (Gröschel et al., 2016). The present assay further allowed semiquantitation of these substrates inside the phagocytes and experimentally demonstrated that active secretion of ESX-1 substrates to the extracellular environment of mycobacteria is a prerequisite for their MHC class II presentation.

BCG and *M. microti* have different RD1 genomic deletions, disabling ESX-1 secretion (Figure S1A). Because immune responses against ESX-1 substrates are important determinants

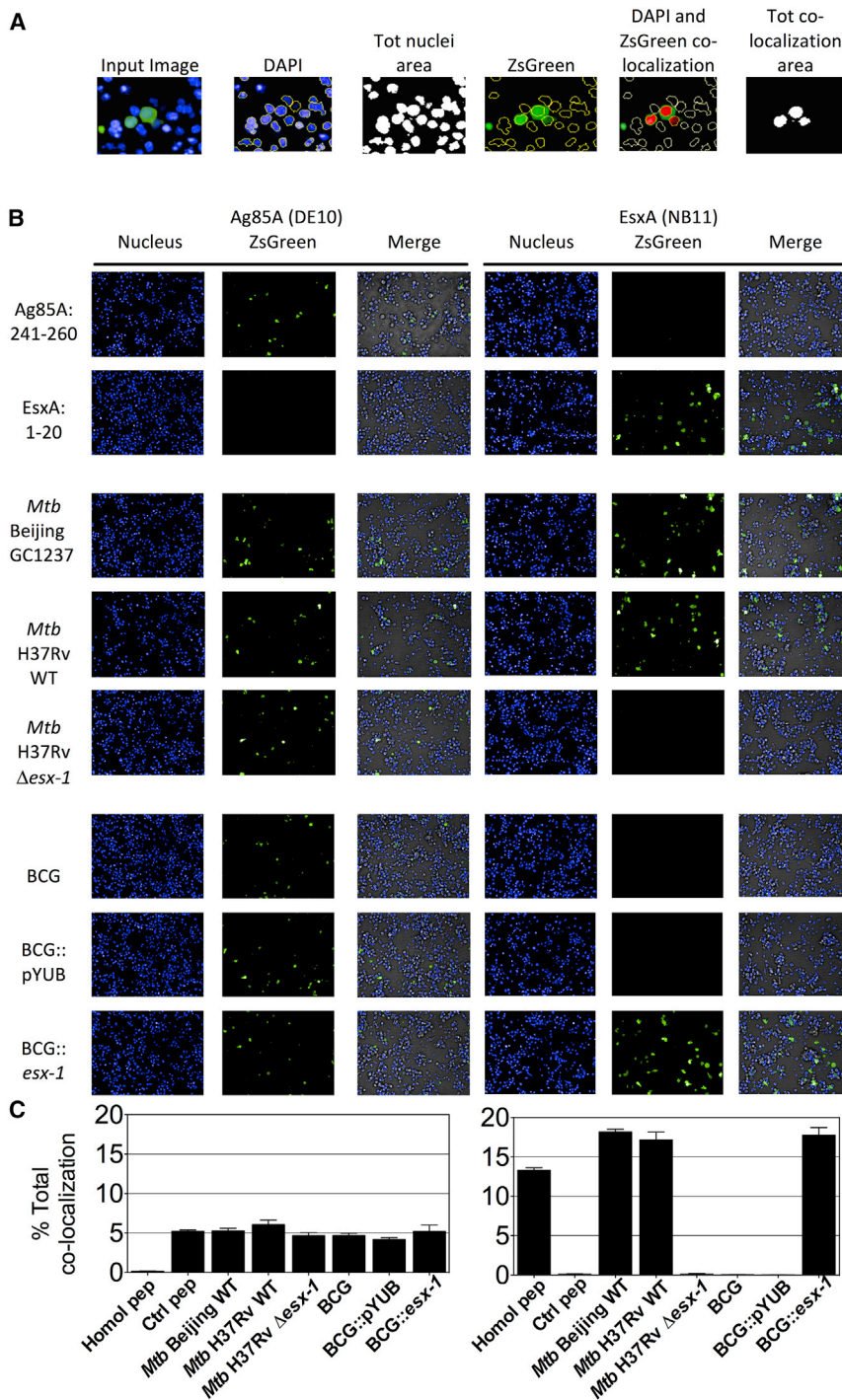


Figure 3. Detection of Intrapagocyte Ag85A/B or EsxA by Use of Reporter T Cell Hybridomas

(A) DCs ($H-2^b$) were loaded with homologous or control peptides or infected with various *esx-1*-proficient or *esx-1*-deficient mycobacteria during 24 hr. Cells were then co-cultured for 24 hr with Ag85A/B- or EsxA-specific T cell hybridomas transduced to express ZsGreen under the *Pmil-2* control. T cell hybridomas were stained with Hoechst before sample acquisition on automated confocal Opera microscopy. Nuclei were segmented by using an intensity threshold of the Hoechst signal collected in the blue channel, and the total nuclei area was quantitated. The surface of the ZsGreen⁺ nuclei area was determined by thresholding the signal intensity on the green channel in the nuclei area. T cell activation was defined and quantitated as an overlap of the ZsGreen⁺ area within the cell nuclei area.

(B) Confocal images (20 \times magnification) of co-cultured Ag85A/B- or EsxA-specific T cells.

(C) Percentages of ZsGreen⁺ T cells were calculated as a general activation index indicative of the total amount of antigen presented to T cells. See also Table S2. Data were pooled from 2 independent experiments, and final results were expressed as the average of 9 images/well in six independent wells.

Error bars represent the SDs of biological co-culture replicates. See also Figure S4 and Tables S2 and S3.

(Figures 5C–5F) (Brodin et al., 2005, 2006; Pym et al., 2002, 2003). The BCG::*esx-1^{Mtb}* or the recently developed live attenuated vaccine candidate BCG::*esx-1^{Mmar}* (Gröschel et al., 2017), harboring the *esx-1* from *M. marinum*, secreted notable levels of ESX-1 substrates inside the phagocytes, yet less than WT *M. bovis* (Figures 5C and 5D). BCG::*esx-1^{Mtb} Δespl, Δrv3878-rv3881*, or Δ *ppe68* mutants were positive for the intraphagocyte secretion of the ESX-1 substrates tested, which is in accordance with observations in axenic cultures (Gröschel et al., 2016). The *M. microti*::*esx-1^{Mtb}* harboring different *esx-1* gene deletions showed that the intraphagocyte secretion of these ESX-1 substrates occurred regardless of the presence of EspI or EspH but depended on the mem-

brane-associated core components EccB₁ or EccCb₁ (Figures 5E and 5F). This result again confirmed that the active export of these substrates outside mycobacteria is critical for their MHC class II presentation.

of vaccine efficacy, restoration of ESX-1 secretion in vaccine candidates is of significant interest (Aguilo et al., 2017; Gröschel et al., 2017; Kupz et al., 2016; Pym et al., 2003). Therefore, we assessed antigenic presentation induced by recombinant BCG or *M. microti* strains, expressing a functional *esx-1^{Mtb}* region (BCG::*esx-1* or *M. microti*::*esx-1*), as well as different *esx-1^{Mtb}* variants in which selected *esx-1* genes had been deleted

The pleiotropic two-component regulatory system Rv0757/Rv758 (PhoP/PhoR) is required for the virulence of *Mtb*, whereby the response transcriptional positive regulator PhoP impacts the

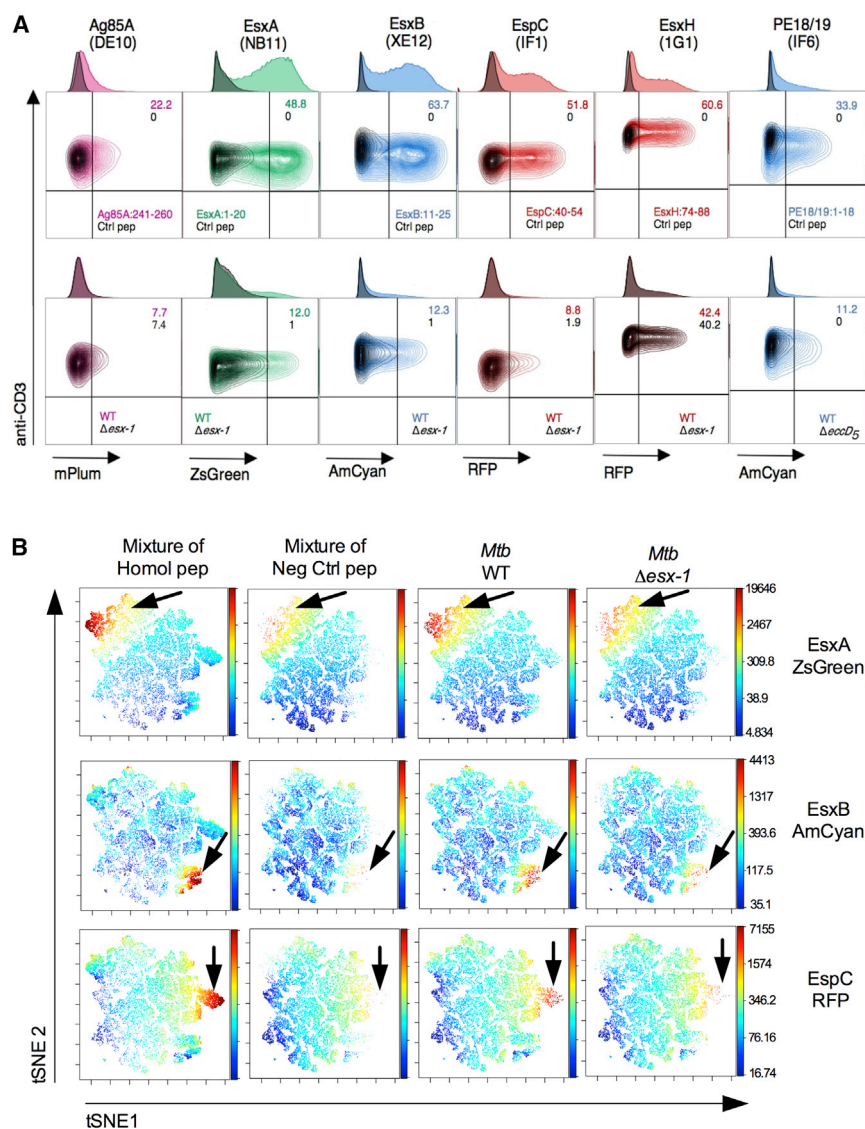


Figure 4. Cytometric Detection of T7S Substrates inside the Phagocytes

(A) Signals produced by T cell hybridomas harboring fluorescent reporters under control of the *Pmil-2* promoter. T cells were analyzed after incubation with DCs loaded with homologous or control peptides (top) or infected with *Mtb* H37Rv WT or mutants (bottom). T cell hybridomas were gated on CD3⁺ CD4⁺ cells and gated out for CD11c⁺ DCs. Numbers on the top right of each contour plot correspond to the percentage of reporter⁺ T cell hybridomas over the total number of CD3⁺ CD4⁺ T cells recovered from the co-culture experiments, with a color code specified at the bottom right of the contour plots. In the bottom right quadrant of plots, the peptides (top) or the mycobacterial strains (bottom) used to pre-condition DCs are indicated. (B) MASSTT deployed to simultaneously detect responses to the EsxA, EsxB, and EspC by the pooled 3 specific hybridomas, co-cultured with C57BL/6 × CBA F1 (H-2^{b/k}) DCs pre-loaded with a mixture of the homologous or negative control peptides or infected with WT or Δ esx-1 *Mtb*, as detected by cytometry and as analyzed using the dimensionality reduction algorithm viSNE on the cells gated on CD3⁺ CD4⁺ T cell populations. See also Figures S4–S6 and Table S3.

ESX-5-Specific MASSTT Assay

The intraphagocytic secretion of ESX-5 substrates in a panel of *Mtb* esx-5 mutants, deleted for various ESX-5 components (Bottai et al., 2012), was investigated by MASSTT using the transduced anti-PE18/19 T cell hybridoma. The PE18/19 MHC class II-restricted presentation was only detected on DCs infected with *Mtb* WT, Δ eccA₅, or Δ esxM, but not with Δ eccD₅ or Δ ppe25-ppe19 mutants (Figure 6A). The PE18/19 presentation was restored in *Mtb* esx-5 mutants complemented with an intact

transcription of ~2% of *Mtb* genes (Gröschel et al., 2016). The MASSTT profiling of *phoP*-deficient (H37Ra, H37Rv Δ phoP) or *phoP*-proficient (H37Rv, H37Ra::phoP) *Mtb* strains was readily detected the PhoP-regulated ESX-1 secretion activity (Frigui et al., 2008), leading to reduced EspC and EsxB detection for *phoP*-deficient strains. In parallel, a strong PhoP-dependent negative regulation of the Tat system was noted, which caused increased Ag85A/B availability for PhoP-inactivated strains (Figure 5G). This effect is likely linked to the non-coding RNA (ncRNA) Mcr7, which dampens translation of the TatC core component in *phoP*-proficient strains (Solans et al., 2014).

The MASSTT assay thus supported the biological relevance of intraphagocyte secretion of ESX-1 and Tat substrates, and their positive or negative regulation, and provided experimental evidence that active secretion of these substrates, in contrast to their sole expression inside the bacilli, is required for initiation of host CD4⁺ T cell activation.

esx-5 locus. All mutants and their complemented counterparts were positive for EsxA as an internal ESX-5-independent positive control. Therefore, these data corroborated our findings on ESX-1, because the active intraphagocyte secretion of the ESX-5 substrates is essential for their antigenic presentation.

Several Clinical Isolates Express Drastically Reduced Amounts of Ag85A/B

Protein secretion levels can vary greatly among isolates from the *Mtb* complex. Examples are lower EsxA secretion due to subtle changes in the PhoPR system (Gonzalo-Asensio et al., 2014) or the defective secretion of a large subset of PE/PPE linked to the deletion of *ppe38* locus (Ates et al., 2018). Here, we investigated a set of clinical *Mtb* isolates, representative of the most prevalent genotypes in France and submitted to the National Reference Centre for TB for drug-resistance characterization and mycobacterial interspersed repetitive-unit-variable number of tandem

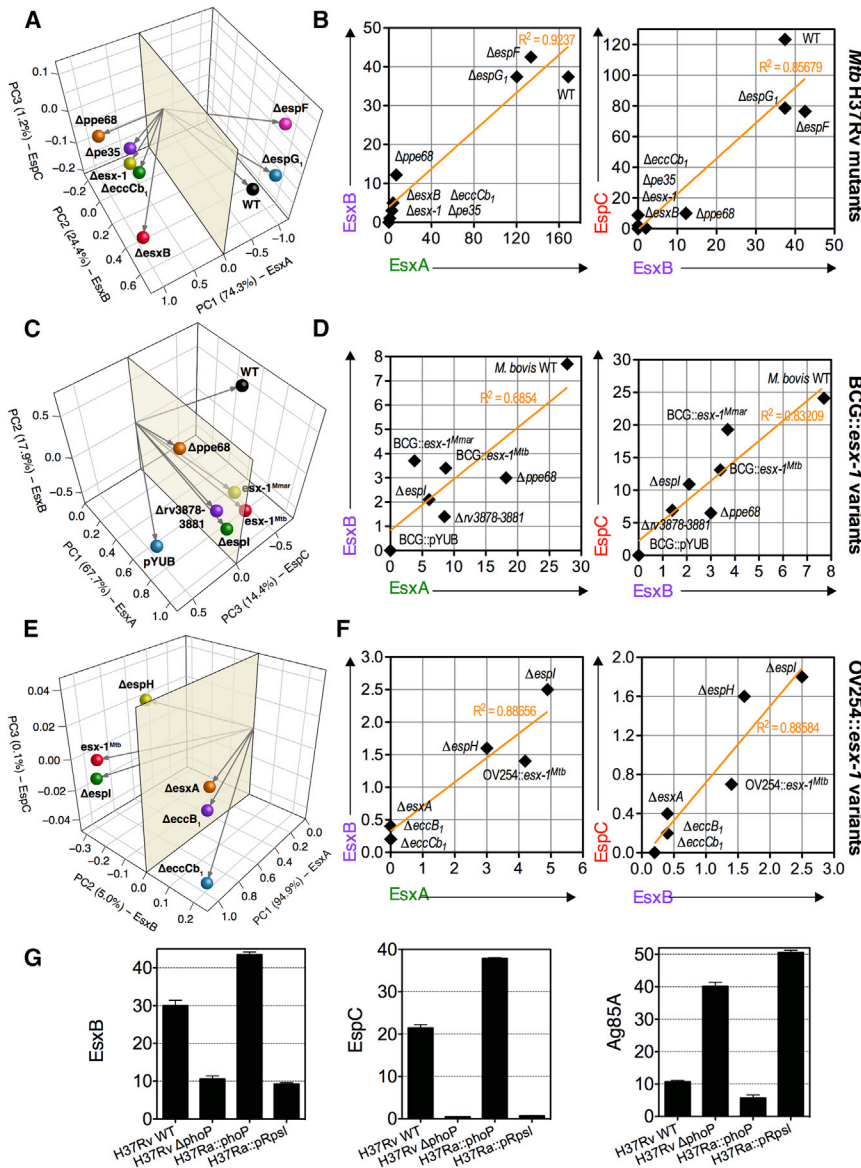


Figure 5. Profiles of EsxA, EsxB, and EspC or Ag85A/B Intraphagocytic Release in a Panel of Mycobacterial Strains

(A, C, and E) PCA projection plots of EsxA, EsxB, and EspC intraphagocyte secretion profiles across a panel of WT, mutant, and complemented *Mtb* (A), BCG (C), and *M. microti* (E) variants. Secretion profiles for each bacterial strain were evaluated as (% reporter⁺ T cells × MFI reporter⁺ T cells)/1,000. (B, D, and F) Correlation of EsxB versus EsxA and EspC versus EsxB intraphagocyte secretion profiles across a panel of WT, mutant, and complemented *Mtb* (B), BCG (D), and *M. microti* (F) variants.

(G) MASSTT ESX-1 or Tat signals for H37Rv/Ra variants, harboring or not harboring a functional PhoP.

Error bars are the SDs of co-culture duplicates. See also Table S4.

The genome sequencing did not establish an immediate link between this phenotype and the SNPs shared by these affected isolates (Table S5). In conclusion, MASSTT can establish the ability of clinical isolates to export mycobacterial effectors and can be extended to larger panels of isolates. This analysis uncovered a reduced capacity of several clinical isolates to secrete Ag85A/B that could not be predicted by genome sequencing and that opens new directions for investigating the reasons for the epidemiological dominance of the highly prevalent Beijing lineage.

Use of MASSTT to Explore the Capacity of Lung Phagocytes to Present Mycobacterial Antigens during Chronic *Mtb* Infection

It is widely accepted that to counteract host adaptive immunity, *Mtb* inhibits

repeat (MIRU-VNTR) genotyping (Table S5) (Allix-Béguet et al., 2008). Three of the strains belonged to *Mtb* lineage 2 (Beijing), while the other three strains belonged to Ural, EAI, or NEW-1 sublineages (Hershberg et al., 2008). These isolates were analyzed by whole-genome sequencing, assessed for SNPs present in the T7S or Tat substrates or cognate core components (Table S5), and MASSTT profiled for EsxA, PE18/19, EsxH, and Ag85A/B (Figures 6B and 6C). The levels of antigen availability differed markedly among the clinical isolates (Figure 6B) and were consistently lower than in H37Rv (Figure 6C). No absence of T7S substrate secretion was noticed in any isolates, despite several SNPs affecting the core components of the cognate secretion systems. However, the 3 Beijing and the NEW1 103788 isolates reproducibly displayed very low amounts of intraphagocyte Ag85A/B (Figures 6C, right panel, and 6D), which distinguished them from the Ural and EAI isolates (Figure 6E).

MHC class II presentation by innate immune cells within the lung granuloma, but not in the draining mediastinal lymph nodes (DMLNs) (Rogerson et al., 2006; Shi et al., 2004). Having established the biological relevance of MASSTT, we used it to evaluate the capacity of phagocytes from lung granuloma to present antigens in comparison to those from DMLNs.

C57BL/6 mice were infected with *Mtb::dsRed*. At 4 weeks post-immunization (p.i.), 2.5% and 16.8% CD11b^{hi} dsRed⁺ cells of total cells were detected in the DMLNs and in the low-density cell fraction recovered from lung granuloma, respectively (Figure 7A). CD11b⁺ cells from mediastinal lymph nodes (MLNs) and the low-density fraction from lung parenchyma of non-infected animals were used as negative controls. Sorted CD11b⁺ cells from DMLNs or granulomas were co-cultured with the transduced anti-EsxA and anti-EspC T cell hybridomas (Figure 7B). Activated ZsGreen⁺ anti-EsxA

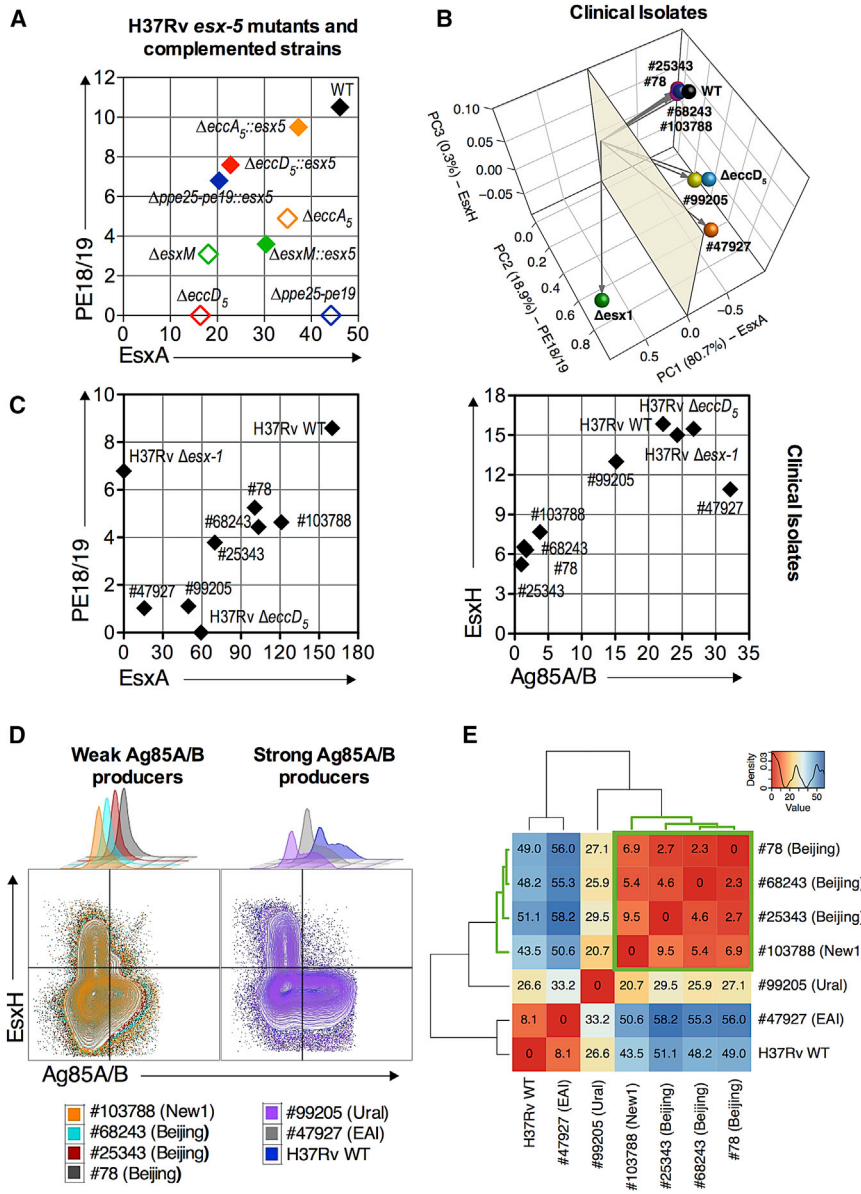


Figure 6. Intraphagocyte Secretion of ESX-3 or ESX-5 Substrates

(A) Intraphagocyte secretion profiles of PE18/19 versus EsxA for various *Mtb* *esx-5* mutants harboring individual deletion of *esx-5* genes or Δ *ppe25-pe19* (open symbols) or complemented mutants (plain symbols), as determined using transduced PE18/19- and EsxA-specific T cells. (B) PCA projection plot of EsxA, PE18/19, EsxH, and Ag85A/B intraphagocyte secretion profiles among *Mtb* H37Rv strains and several clinical isolates detailed in Table S5. Secretion profiles for each bacterial strain were evaluated as (% reporter⁺ T cells × MFI reporter⁺ T cells)/1,000. (C) Intraphagocyte secretion profiles of PE18/19 versus EsxA or EsxH versus Ag85A/B by several *Mtb* clinical isolates compared to *Mtb* H37Rv WT. (D) Cytometric overlaid contour blots of EsxH-versus Ag85A/B-specific signals for *Mtb* groups with low or high intraphagocyte Ag85A/B secretion. (E) Hierarchical clustering of the Euclidean distances on the intraphagocyte Ag85A/B secretion signal retrieved upon infection with *Mtb* H37Rv or clinical isolates. See also Tables S4 and S5.

DISCUSSION

The comprehensive appraisal of the key virulence and immunogenicity proteins secreted by mycobacterial ESX secretion systems can be hindered by their high sequence similarities. Here, we demonstrate the feasibility of selecting highly sensitive MHC class II-restricted TCRs with strongly discriminative capacity that recognize individual members of these families in an exclusive manner. So far, exclusive and individual detection of selected members of the PE/PEP protein families had not been possible using immunological tools because of extensive gene duplication events and the tremendous amount of shared T cell or

T cells were readily detected at up to 12.8% in the granuloma-derived CD11b⁺ cells, within total CD3⁺ T cells relative to 3.8% for the MLN-derived cells and 0% in the negative co-culture controls (Figure 7B). More than 9% of activated RFP⁺ anti-EspC T cells, within total CD3⁺ T cells, were detected in both granuloma- and DMLN-derived cells (Figures 7B and 7C). At the chronic phase of infection, the MHC class II presentation of the representative antigens EsxA and EspC still occurs and remains at least comparable for phagocytes from the lung granuloma or DMLN. Therefore, in contrast to the dogma (Rogerson et al., 2006; Shi et al., 2004), our data suggest that *Mtb* antigen presentation via MHC class II by innate immune cells of the lung granuloma remains detectable and that it can contribute to the local activation of the host CD4⁺ T cell effectors.

B cell epitopes that lead to cross-reactivities (Sayes et al., 2012; Vordermeier et al., 2012). We provide the proof of concept that T cells bearing highly discriminative TCRs can be used to explore the topology of ESX substrates in the sub-mycobacterial compartments. Furthermore, we observed that the enigmatic ESX-5-associated PE18/19 protective antigens are localized in the cell wall and culture supernatants of *Mtb* and *M. marinum* in an ESX-5-dependent manner. This is an important biological finding considering the proposed role for PE19 in cell wall permeability and virulence. This also highlights the advantages of this assay over conventional biochemical immunoblotting or mass spectrometry, which were unsuccessful in PE18/19 topography (Ates et al., 2015; Ramakrishnan et al., 2015). The presence of PE18/19 in cell wall and secreted fractions and the largely reduced virulence

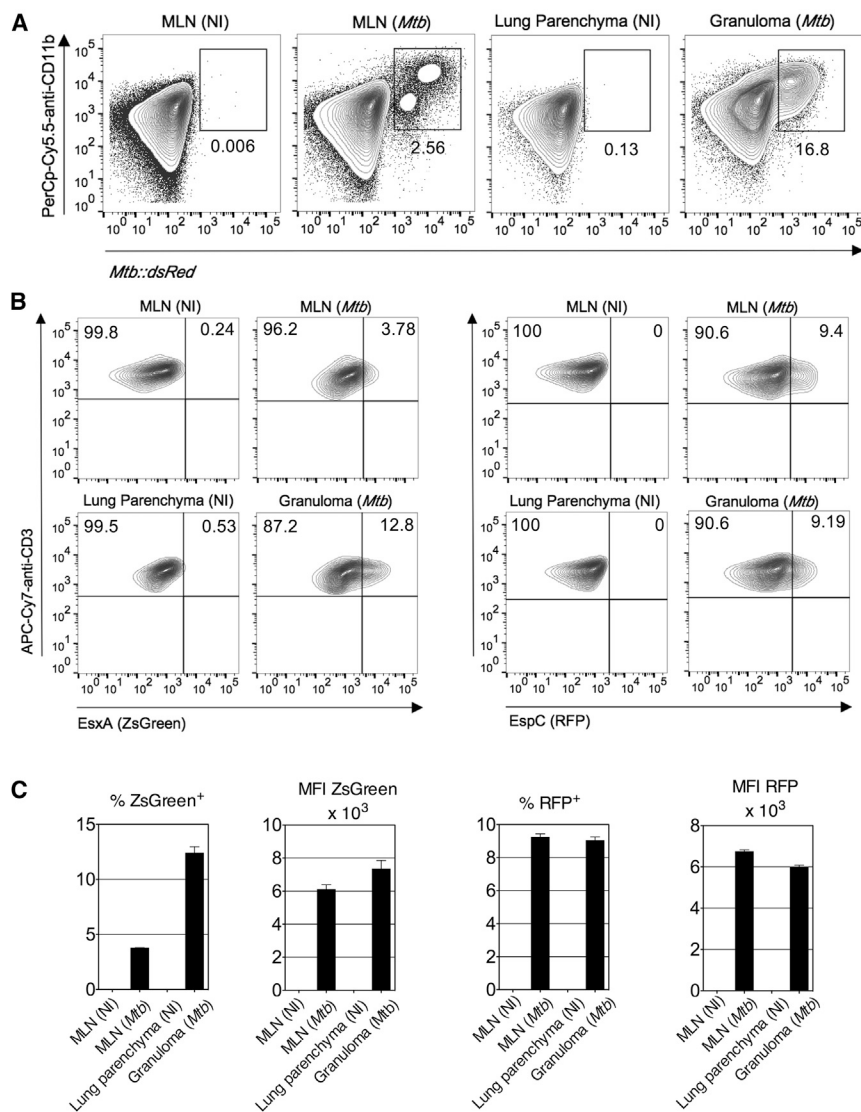


Figure 7. Comparative Capacity of Antigen Presentation by Phagocytes from the Lung Granuloma or MLN of *Mtb*-Infected Mice

C57BL/6 mice (n = 2/group) were left untreated or infected with *Mtb::dsRed*.

(A) At 4 weeks post-infection, total cells from MLN or low-density cells isolated from the lung granuloma were analyzed for the intracellular *Mtb::dsRed* content. MLN or low-density cells from the lung parenchyma from non-infected (NI) mice were used as negative controls. Percentages of dsRed⁺ CD11b^{hi} cells are indicated in each dot plot.

(B) CD11b⁺ cells were sorted from MLN, lung granuloma, or lung parenchyma and co-cultured with transduced EsxA- or EspC-specific T cells during the 24 hr before surface staining and cytometric analyses.

(C) Percentages or MFI of the reporter⁺ T cells from a representative experiment.

Error bars are the SDs of technical replicates.

of strain *Mtb*Δ*ppe25-pe19* (Bottai et al., 2012) strongly suggest a direct interaction between these PE proteins and the host (pattern recognition) receptors. In contrast, with this T cell-based approach, EsxA and EsxB were detected not in *Mtb* membrane or cell wall fractions but only in their culture supernatants, suggesting that they essentially exert their functions as soluble released factors (Simeone et al., 2016).

We generated a panel of transduced T cell hybridomas emitting specific reporter signals after the detection of epitopes derived from ESX or Tat substrates. With such tools, we developed the MASSTT approach, enabling measurement of intraphagocyte secretion of T7S substrates, which accounts for the possible influences of the host-pathogen interplay on these secretion systems, reported to be regulated tightly by the host environment (Abramovitch et al., 2011; Ates et al., 2016; Queval et al., 2017).

MASSTT profiling of mutants modified in selected genes inside the *esx-1* region of different genetic backgrounds (*Mtb*,

machinery components demonstrated that active secretion of these ESX-1 substrates is a prerequisite for their access to the host MHC class II pathway. This information is crucial for the capacity of recombinant live attenuated vaccines to trigger CD4⁺ T cell responses, considered key elements of the anti-mycobacterial adaptive immune arsenal.

Based on ESX-5-specific MASSTT, the PE18/19 intraphagocyte secretion fully depended on the EccD₅-containing apparatus, while deletion of EccA₅, the cytosolic ESX-5-associated ring-shaped hexameric ATPase, did not abolish this secretion. However, the *Mtb* Δ*eccA5* mutant showed quantitatively decreased PE18/19 secretion, suggesting a partial or redundant contribution of EccA₅ (Ates et al., 2016).

Because secretion defects can be reliably measured as altered antigenic presentation, we MASSTT profiled a panel of *Mtb* clinical isolates. The parallel genome sequencing of these strains allowed assessment of the impact of detected SNPs in the tested substrates or their cognate secretion systems. We

show that several non-synonymous SNPs present in the genes encoding the ESX-3 and ESX-5 core machineries did not impair secretion by these systems. In contrast, a clear reduction in Ag85A/B availability was found specifically in the tested lineage 2 *Mtb* strains (also known as Beijing strains), which was apparently not linked to polymorphisms in the genes encoding Ag85A/B or the TatABC secretion components. However, a potential impact of the PhoP-regulated ncRNA Mcr7 modulating the Tat system (Solans et al., 2014) cannot be excluded and will be the subject of future investigations. The reduced Ag85A/B expression by lineage 2 isolates may have biological implications, because Ag85 immunogens are present in multiple vaccine candidates (Fletcher and Schrager, 2016). Our results, not predictable by classical antigen variation studies based on genome sequencing, suggest that Ag85-based immunogens might not be efficient for the use against all clinical isolates. These results highlight the value of MASSTT to screen the immunogenicity of clinical *Mtb* isolates in a physiologically relevant intracellular environment, which can now be extended to larger panels of isolates.

Finally, we used the MASSTT approach to explore antigenic presentation capacity of the innate immune cells from lung granuloma at the chronic phase of infection. The blockade of MHC class II presentation of the lung granuloma phagocytes has often been evoked as constituting a major mechanism developed by *Mtb* to disarm host CD4⁺ T cell immunity. We demonstrate that CD11b⁺ cells from the pulmonary granulomas were as competent as their counterparts isolated from DMLNs at presenting MHC class II epitopes from mycobacterial antigens. Therefore, in contrast to previous reports (Rogerson et al., 2006; Shi et al., 2004), our results provide strong experimental evidence that MHC class II antigenic presentation by innate immune cells remains active in the lung granulomas.

Considering the prominent roles of bacterial secretion systems in immunity and pathogenesis, the semiquantitative intraphagocyte detection of their substrates by MASSTT will have numerous applications, not only in the study of the functional mechanisms of these systems but also in advanced microscopy or high-throughput screening in new approaches of TB drug discovery (Christophe et al., 2009) or for the immunogenicity prediction of new TB vaccine candidates.

EXPERIMENTAL PROCEDURES

Mycobacteria

All mycobacterial strains were grown to the exponential phase in Dubos broth, complemented with albumin, dextrose, and catalase (ADC; Difco, Le Pont-de-Claix, France). *M. marinum* isolates were pre-cultured in 7H9 medium supplemented with ADC. Clinical isolates were grown in Dubos broth, complemented with oleic albumin, dextrose, and catalase (OADC, Difco). For infection experiments using the confocal microscopy, mycobacteria were grown in 7H9 medium supplemented with 10% OADC, 0.2% glycerol, and 0.05% Tween 80 (Sigma-Aldrich) and with 50 µg/mL Hygromycin B (Invitrogen) for BCG::esx-1. Before infection, bacilli were washed with PBS, resuspended in RPMI (Gibco) containing 5% heat-inactivated fetal bovine serum (FBS, Gibco), and centrifuged at 700 rpm for 2 min to remove aggregates. Bacterial titer of the suspension was determined by optical density 600 (OD₆₀₀) measuring. All experiments with pathogenic mycobacteria of the *Mtb* complex were performed in Bio Safety Level 3 (BSL3), in accordance with the hygiene and security recommendations of Institut Pasteur.

Peptides and Pepsans

The synthetic peptides that harbor *Mtb* MHC class II-restricted epitopes were synthesized by PolyPeptide (Strasbourg, France) and were reconstituted in H₂O containing 5% DMSO (Sigma-Aldrich). The Pepsan composed of peptides from EspC (thirty-one 15-mers, offset by 4 AA) were synthesized by Mimotope (Melbourne, Australia).

Generation of T Cell Hybridomas

T cell hybridomas specific to EsxA:1–20, EsxH:74–88, Ag85A:101–120, or Ag85A:241–260 sequences that harbor T cell epitopes restricted by MHC class II were generated previously (Frigui et al., 2008; Majlessi et al., 2006). Those specific to EsxB:11–25, EspC:40–54, or PE18/19:1–18 were generated, respectively, from C3H (H-2^b) or C57BL/6 (H-2^b) mice immunized subcutaneously (s.c.) with 50 µg/mouse of the synthetic peptide formulated in Freund's incomplete adjuvant. Ten days post-immunization, splenocytes were stimulated with 10 µg/mL of specific peptide in RPMI containing 10% FBS. Following 4 days of incubation, viable cells were recovered on Lympholyte M (Cedarlane Laboratories) and fused at a ratio of 1:1 with BW51-47 thymoma cells using polyethylene glycol 1500 (Roche Diagnostics), as previously described (Majlessi et al., 2006). Two weeks later, hybridomas proliferating in positive wells were amplified individually and screened for their capacity to release IL-2 upon recognition of bone marrow-derived dendritic cells (BM-DCs) loaded with 1 µg/mL of homologous peptide, but not negative control peptide. The selected T cells were then screened on BM-DCs infected at an MOI of 1 with *Mtb* WT; *Mtb* deficient for the RD1 region (Hsu et al., 2003), referred to as Δesx-1 in this paper; or Δppe25-pe19 or ΔeccD₅ (Bottai et al., 2012) *Mtb* mutants. The presence of IL-2 in the co-culture supernatants was assessed by ELISA after overnight incubation.

Confocal Microscopy

Isogenic BM-DCs were seeded in 96-well plates at 1×10^5 cells/well in 100 µL of RPMI containing 10% FBS. After overnight incubation, cells were loaded with 1 µg/mL of homologous or control peptides or infected with mycobacterial strains (MOI = 2). After a 2 hr incubation, DCs were washed and co-cultured with 5×10^4 transduced anti-Ag85A/B or anti-EsxA T cell hybridomas. After 24 hr incubation, the non-adherent T cells were transferred into new 96-well Greiner plates. Cell nuclei were stained with 10 µg/mL of Hoechst 33342 (Sigma-Aldrich) for 30 min at 37°C. Image acquisitions were performed on an automated fluorescence confocal microscope Opera (PerkinElmer) using a 20× water immersion lens. Hoechst-labeled T cell nuclei were detected using a 405-nm excitation laser coupled with a 450/50 detection filter, and ZsGreen⁺ antigen-activated T cells were detected using a 488-nm laser coupled with a 540/75 detection filter. T cells were detected using the transmitted light coupled with a 690-nm filter (bright field). Nine fields/well were recorded. Each image was processed using an in-house, multiparameter script developed with the Columbus system (v.2.3.1), as detailed in Table S1.

MASSTT Assay

Isogenic BM-DCs were plated at 1×10^6 cells/mL/well in 24-well plates in RPMI 1640 containing 5% FBS. After overnight incubation, cells were infected with mycobacteria (MOI = 1) or were loaded with 1 µg/mL of homologous or control peptides. At 24 hr post-infection 2.5×10^5 cells/well of each transduced T cell hybridoma were added. After 24 hr of co-culture, cells were harvested and stained with APC-eF780-anti-CD3_ε and PerCP-Cy5.5-anti-CD4 monoclonal antibodies (mAbs) at 4°C. When indicated, APC-anti-CD11b mAb was also added to gate out the DC. The stained cells were washed twice with PBS containing 3% FBS and 0.1% NaN₃ and fixed with 4% paraformaldehyde overnight at 4°C. T cells transduced with LV vectors harboring genes coding for individual fluorochromes under the constitutive EF1α promoter (Figure S4, right) were used to set up the cytometer. Cells were acquired in an LSR Fortessa flow cytometer system using BD FACSDiva software (BD Biosciences). Cytometric data were analyzed using FlowJo software (Tree Star, OR, USA) or the visNE algorithm in Cytobank. PCA was performed by using the R function prcomp (center TRUE; scale. TRUE) on intraphagocyte secretion profiles determined for each bacterial strain as (% reporter⁺ T cells × MFI reporter⁺ T cells)/1,000. For hierarchical clustering of *Mtb* clinical isolates according to intraphagocyte Ag85A/B secretion, Euclidean distances were

computed on regularized-logarithm transformed fluorescence intensities (Love et al., 2014) and plotted by using the function heatmap.2 from the R package gplots.

Whole-Genome Sequencing

DNA extraction was performed using the cetyltrimethylammonium bromide (CTAB) method as described (Lemaître et al., 1998). Libraries were constructed by using the Nextera XT DNA Sample Preparation Kit (Illumina) following the manufacturer's instructions. 150-bp paired-end reads with a mean insert size of 1 kb were generated and analyzed by GenoScreen (Lille, France) using an Illumina MiSeq device (median sequencing depth of 53.8×). Sequencing pairs were mapped against the *Mtb* H37Rv genome (GenBank: NC_000962.3) using Bowtie2 (Langmead and Salzberg, 2012). After mapping, SNPs were called using SAMtools (Li et al., 2009). Regions corresponding to the highly repeated regions PE-PPE-PGRS were filtered out to ensure confidence in SNP calling. The accession number for the sequencing data reported in this paper is ENA (European Nucleotide Archive): PRJEB23484.

Mice, Infection with *Mtb*, and Preparation of Cell Suspensions

C57BL/6 (H-2^b), BALB/c (H-2^d), C3H (H-2^k), and C57BL/6 × CBA (H-2^{b/k}) female mice were purchased from Janvier (Le Genest-Saint-Isle, France). For *ex vivo* antigen presentation assay, 10-week-old female C57BL/6 (H-2^b) mice were infected with ~200 colony-forming units (CFUs) of *Mtb*::ds-Red H37Rv via aerosol. Mice were placed in an isolator in BSL3 facilities at Institut Pasteur. Four weeks later, DMLNs or lung granulomas were removed, pooled, and disaggregated by treatment with 400 U/mL of type IV collagenase and DNase I (Roche). After 45 min of incubation at 37°C, single-cell suspensions were prepared by gentle squeezing and passage through 100-µm nylon filters (Cell Strainer; BD Falcon). Cells from granulomas were enriched in low-density cells by Optiprep gradient. CD11b⁺ cells were enriched from these cell fractions by positive magnetic sorting using microbeads (Miltenyi) and were used in MASSTT in co-cultures with transduced T cell hybridomas for *ex vivo* antigen presentation assay, as described earlier. Investigations in mice were performed in accordance with the European and French guidelines (Directive 86/609/CEE and Decree 87-848 of 19 October 1987) after approval by the Institut Pasteur Safety, Animal Care and Use Committee under local ethical committee protocol agreements CETEA 2013-0036 and CETEA 2012-0005.

SUPPLEMENTAL INFORMATION

Supplemental Information includes Supplemental Experimental Procedures, six figures, and five tables and can be found with this article online at <https://doi.org/10.1016/j.celrep.2018.03.125>.

ACKNOWLEDGMENTS

The authors thank Françoise Guinet (Institut Pasteur) for critical reading of the manuscript, Philippe Souk (Institut Pasteur) for advice concerning LV vector construction and titration, and Ida Rosenkrands (Statens Serum Institut, Copenhagen, Denmark) for the gift of the anti-SigA antibody. We acknowledge The Technology Core of the Center for Translational Science (CRT) at Institut Pasteur for support in conducting this study, in particular Sophie Novault and Pierre-Henri Commere of the Flow Cytometry facility. We are grateful to Carlos Martin (University of Zaragoza, Spain) for sharing Beijing GC1237 and *ΔphoP Mtb* strains and to Jeffery Chen (École Polytechnique Fédérale de Lausanne, Switzerland; University of Saskatchewan, Canada) for the *ΔespA* strain. This work was supported in part by the Institut Pasteur (PTR 441 to L.M. and P.B.), the Agence Nationale de Recherche (ANR-14-CE08-0017 to L.M. and P.B. and ANR-14-JAMR-001-02, ANR-10-LABX-62-IBEID, and ANR-16-CE35-0009 to R.B.), the European Union's Research and Innovation Program (MM4TB 260872 to R.B. and P.B., TBVAC2020 643381 to R.B. and P.C., and ERC-STG INTRACELLTB 260901 to P.B.), grants from the Fondation pour la Recherche Médicale (DEQ20130326471 and SPF20160936136 to R.B. and M.O.), and contributions from the Feder (12001407 D-AL), Equipex Imaginex BioMed (ANR-10-EQPX-04-01), and the Région Nord Pas de Calais (Convention 12000080) to P.B.

AUTHOR CONTRIBUTIONS

F.S. designed, performed, and analyzed the experiments. C.B. constructed LV vectors. L.S.A. performed mycobacterial fractionation and western blot analysis and wrote the paper. N.D. and O.-R.S. performed Opera confocal experiments. M.O. performed bioinformatics analyses. F.L.C. designed mycobacterial fractionation. M.I.G. generated the anti-EsxB T cell hybridoma and critically read the paper. W.F. maintained mycobacterial collection and performed *Mtb* aerosol challenges. F.B. and W.S. provided the clinical isolates and their whole-genome sequences. R.L.-M. performed cytometric viSNE analyses. D.B. designed experiments and provided several *esx-1* and all *esx-5* mutants. P.B. designed, performed, and analyzed the confocal experiments. P.C. designed the LV vectors. R.B. conceptualized and designed experiments, analyzed the results, and wrote the paper. L.M. conceptualized, designed, and performed the experiments; analyzed the data; and wrote the paper.

DECLARATION OF INTERESTS

The authors declare no competing interests.

Received: January 4, 2018

Revised: February 16, 2018

Accepted: March 26, 2018

Published: April 24, 2018

REFERENCES

- Abramovitch, R.B., Rohde, K.H., Hsu, F.F., and Russell, D.G. (2011). *aprABC*: a *Mycobacterium tuberculosis* complex-specific locus that modulates pH-driven adaptation to the macrophage phagosome. *Mol. Microbiol.* **80**, 678–694.
- Aguilo, N., Gonzalo-Asensio, J., Alvarez-Arguedas, S., Marinova, D., Gomez, A.B., Uranga, S., Spallek, R., Singh, M., Audran, R., Spertini, F., and Martin, C. (2017). Reactogenicity to major tuberculosis antigens absent in BCG is linked to improved protection against *Mycobacterium tuberculosis*. *Nat. Commun.* **8**, 16085.
- Alix-Béguec, C., Harmsen, D., Weniger, T., Supply, P., and Niemann, S. (2008). Evaluation and strategy for use of MIRU-VNTRplus, a multifunctional database for online analysis of genotyping data and phylogenetic identification of *Mycobacterium tuberculosis* complex isolates. *J. Clin. Microbiol.* **46**, 2692–2699.
- Altschul, S.F., Madden, T.L., Schäffer, A.A., Zhang, J., Zhang, Z., Miller, W., and Lipman, D.J. (1997). Gapped BLAST and PSI-BLAST: a new generation of protein database search programs. *Nucleic Acids Res.* **25**, 3389–3402.
- Amir, el-A.D., Davis, K.L., Tadmor, M.D., Simonds, E.F., Levine, J.H., Bendall, S.C., Shenfeld, D.K., Krishnaswamy, S., Nolan, G.P., and Pe'er, D. (2013). viSNE enables visualization of high dimensional single-cell data and reveals phenotypic heterogeneity of leukemia. *Nat Biotechnol.* **31**, 545–552.
- Ates, L.S., Ummels, R., Commandeur, S., van de Weerd, R., Sparrius, M., Weerdenburg, E., Alber, M., Kalscheuer, R., Piersma, S.R., Abdallah, A.M., et al. (2015). Essential role of the ESX-5 secretion system in outer membrane permeability of pathogenic mycobacteria. *PLoS Genet.* **11**, e1005190.
- Ates, L.S., Houben, E.N., and Bitter, W. (2016). Type VII secretion: a highly versatile secretion system. *Microbiol. Spectr.* **4**, VMBF-0011-2015.
- Ates, L.S., Dippenaar, A., Ummels, R., Piersma, S.R., van der Woude, A.D., van der Kuij, K., le Chevalier, F., Mata-Espinosa, D., Barrios-Payán, J., Marquina-Castillo, B., et al. (2018). Mutations in *ppe38* block PE_PGRS secretion and increase virulence of *Mycobacterium tuberculosis*. *Nat. Microbiol.* **3**, 181–188.
- Beckham, K.S., Ciccarelli, L., Bunduc, C.M., Mertens, H.D., Ummels, R., Lugmayr, W., Mayr, J., Rettel, M., Savitski, M.M., Svergun, D.I., et al. (2017). Structure of the mycobacterial ESX-5 type VII secretion system membrane complex by single-particle analysis. *Nat. Microbiol.* **2**, 17047.
- Betts, J.C., Dodson, P., Quan, S., Lewis, A.P., Thomas, P.J., Duncan, K., and McAdam, R.A. (2000). Comparison of the proteome of *Mycobacterium*

- tuberculosis* strain H37Rv with clinical isolate CDC 1551. *Microbiology* **146**, 3205–3216.
- Bottai, D., Di Luca, M., Majlessi, L., Frigui, W., Simeone, R., Sayes, F., Bitter, W., Brennan, M.J., Leclerc, C., Batoni, G., et al. (2012). Disruption of the ESX-5 system of *Mycobacterium tuberculosis* causes loss of PPE protein secretion, reduction of cell wall integrity and strong attenuation. *Mol. Microbiol.* **83**, 1195–1209.
- Brodin, P., de Jonge, M.I., Majlessi, L., Leclerc, C., Nilges, M., Cole, S.T., and Brosch, R. (2005). Functional analysis of early secreted antigenic target-6, the dominant T-cell antigen of *Mycobacterium tuberculosis*, reveals key residues involved in secretion, complex formation, virulence, and immunogenicity. *J. Biol. Chem.* **280**, 33953–33959.
- Brodin, P., Majlessi, L., Marsollier, L., de Jonge, M.I., Bottai, D., Demangel, C., Hinds, J., Neyrolles, O., Butcher, P.D., Leclerc, C., et al. (2006). Dissection of ESAT-6 system 1 of *Mycobacterium tuberculosis* and impact on immunogenicity and virulence. *Infect. Immun.* **74**, 88–98.
- Champion, P.A. (2013). Disconnecting *in vitro* ESX-1 secretion from mycobacterial virulence. *J. Bacteriol.* **195**, 5418–5420.
- Chen, J.M., Zhang, M., Rybniker, J., Basterra, L., Dhar, N., Tischler, A.D., Pojer, F., and Cole, S.T. (2013). Phenotypic profiling of *Mycobacterium tuberculosis* EspA point mutants reveals that blockage of ESAT-6 and CFP-10 secretion *in vitro* does not always correlate with attenuation of virulence. *J. Bacteriol.* **195**, 5421–5430.
- Christophe, T., Jackson, M., Jeon, H.K., Fenistein, D., Contreras-Dominguez, M., Kim, J., Genovesio, A., Carralot, J.P., Ewann, F., Kim, E.H., et al. (2009). High content screening identifies decaprenyl-phosphoribose 2' epimerase as a target for intracellular antimycobacterial inhibitors. *PLoS Pathog.* **5**, e1000645.
- Daleke, M.H., Cascioferro, A., de Punder, K., Ummels, R., Abdallah, A.M., van der Wel, N., Peters, P.J., Luirink, J., Manganelli, R., and Bitter, W. (2011). Conserved Pro-Glu (PE) and Pro-Pro-Glu (PPE) protein domains target LipY lipases of pathogenic mycobacteria to the cell surface via the ESX-5 pathway. *J. Biol. Chem.* **286**, 19024–19034.
- Deane, J.E., Abrusci, P., Johnson, S., and Lea, S.M. (2010). Timing is everything: the regulation of type III secretion. *Cell. Mol. Life Sci.* **67**, 1065–1075.
- Dewoody, R.S., Merritt, P.M., and Marketon, M.M. (2013). Regulation of the Yersinia type III secretion system: traffic control. *Front. Cell. Infect. Microbiol.* **3**, 4.
- Di Luca, M., Bottai, D., Batoni, G., Orgeur, M., Aulicino, A., Counoupas, C., Campa, M., Brosch, R., and Esin, S. (2012). The ESX-5 associated eccB-EccC locus is essential for *Mycobacterium tuberculosis* viability. *PLoS ONE* **7**, e52059.
- Dumas, E., Christina Boritsch, E., Vandenbogaert, M., Rodríguez de la Vega, R.C., Thiberge, J.M., Caro, V., Gaillard, J.L., Heym, B., Girard-Misguich, F., Brosch, R., and Sapriel, G. (2016). Mycobacterial pan-genome analysis suggests important role of plasmids in the radiation of type VII secretion systems. *Genome Biol. Evol.* **8**, 387–402.
- Ferris, H.U., and Minamino, T. (2006). Flipping the switch: bringing order to flagellar assembly. *Trends Microbiol.* **14**, 519–526.
- Fishbein, S., van Wyk, N., Warren, R.M., and Sampson, S.L. (2015). Phylogeny to function: PE/PPE protein evolution and impact on *Mycobacterium tuberculosis* pathogenicity. *Mol. Microbiol.* **96**, 901–916.
- Fletcher, H.A., and Schrager, L. (2016). TB vaccine development and the End TB Strategy: importance and current status. *Trans. R. Soc. Trop. Med. Hyg.* **110**, 212–218.
- Frigui, W., Bottai, D., Majlessi, L., Monot, M., Josselin, E., Brodin, P., Garnier, T., Gicquel, B., Martin, C., Leclerc, C., et al. (2008). Control of *M. tuberculosis* ESAT-6 secretion and specific T cell recognition by PhoP. *PLoS Pathog.* **4**, e33.
- Gey van Pittius, N.C., Sampson, S.L., Lee, H., Kim, Y., van Helden, P.D., and Warren, R.M. (2006). Evolution and expansion of the *Mycobacterium tuberculosis* PE and PPE multigene families and their association with the duplication of the ESAT-6 (*esx*) gene cluster regions. *BMC Evol. Biol.* **6**, 95.
- Gonzalo-Asensio, J., Malaga, W., Pawlik, A., Astarie-Dequeker, C., Passemar, C., Moreau, F., Laval, F., Daffé, M., Martin, C., Brosch, R., and Guilhot, C. (2014). Evolutionary history of tuberculosis shaped by conserved mutations in the PhoPR virulence regulator. *Proc. Natl. Acad. Sci. USA* **111**, 11491–11496.
- Gröschel, M.I., Sayes, F., Simeone, R., Majlessi, L., and Brosch, R. (2016). ESX secretion systems: mycobacterial evolution to counter host immunity. *Nat. Rev. Microbiol.* **14**, 677–691.
- Gröschel, M.I., Sayes, F., Shin, S.J., Frigui, W., Pawlik, A., Orgeur, M., Canetti, R., Honoré, N., Simeone, R., van der Werf, T.S., et al. (2017). Recombinant BCG expressing ESX-1 of *Mycobacterium marinum* combines low virulence with cytosolic immune signaling and improved TB protection. *Cell Rep.* **18**, 2752–2765.
- Hershberg, R., Lipatov, M., Small, P.M., Sheffer, H., Niemann, S., Homolka, S., Roach, J.C., Kremer, K., Petrov, D.A., Feldman, M.W., and Gagneux, S. (2008). High functional diversity in *Mycobacterium tuberculosis* driven by genetic drift and human demography. *PLoS Biol.* **6**, e311.
- Hervas-Stubbs, S., Majlessi, L., Simsova, M., Morova, J., Rojas, M.J., Nouzé, C., Brodin, P., Sebo, P., and Leclerc, C. (2006). High frequency of CD4+ T cells specific for the TB10.4 protein correlates with protection against *Mycobacterium tuberculosis* infection. *Infect. Immun.* **74**, 3396–3407.
- Houben, E.N., Bestebroer, J., Ummels, R., Wilson, L., Piersma, S.R., Jiménez, C.R., Ottenhoff, T.H., Luirink, J., and Bitter, W. (2012). Composition of the type VII secretion system membrane complex. *Mol. Microbiol.* **86**, 472–484.
- Hsu, T., Hingley-Wilson, S.M., Chen, B., Chen, M., Dai, A.Z., Morin, P.M., Marks, C.B., Padiyar, J., Goulding, C., Gingery, M., et al. (2003). The primary mechanism of attenuation of bacillus Calmette-Guérin is a loss of secreted lytic function required for invasion of lung interstitial tissue. *Proc. Natl. Acad. Sci. USA* **100**, 12420–12425.
- Kamath, A.B., Woodworth, J., Xiong, X., Taylor, C., Weng, Y., and Behar, S.M. (2004). Cytolytic CD8+ T cells recognizing CFP10 are recruited to the lung after *Mycobacterium tuberculosis* infection. *J. Exp. Med.* **200**, 1479–1489.
- Kupz, A., Zedler, U., Stäber, M., Perdomo, C., Dorhoi, A., Brosch, R., and Kaufmann, S.H. (2016). ESAT-6-dependent cytosolic pattern recognition drives noncognate tuberculosis control *in vivo*. *J. Clin. Invest.* **126**, 2109–2122.
- Langmead, B., and Salzberg, S.L. (2012). Fast gapped-read alignment with Bowtie 2. *Nat. Methods* **9**, 357–359.
- Lemaître, N., Sougakoff, W., Truffot-Pernot, C., Cambau, E., Derenne, J.P., Bricaire, F., Grosset, J., and Jarlier, V. (1998). Use of DNA fingerprinting for primary surveillance of nosocomial tuberculosis in a large urban hospital: detection of outbreaks in homeless people and migrant workers. *Int. J. Tuberc. Lung Dis.* **2**, 390–396.
- Li, H., Handsaker, B., Wysoker, A., Fennell, T., Ruan, J., Homer, N., Marth, G., Abecasis, G., and Durbin, R.; 1000 Genome Project Data Processing Subgroup (2009). The Sequence Alignment/Map format and SAMtools. *Bioinformatics* **25**, 2078–2079.
- Love, M.I., Huber, W., and Anders, S. (2014). Moderated estimation of fold change and dispersion for RNA-seq data with DESeq2. *Genome Biol.* **15**, 550.
- Majlessi, L., Simsova, M., Jarvis, Z., Brodin, P., Rojas, M.J., Bauche, C., Nouzé, C., Ladant, D., Cole, S.T., Sebo, P., and Leclerc, C. (2006). An increase in antimycobacterial Th1-cell responses by prime-boost protocols of immunization does not enhance protection against tuberculosis. *Infect. Immun.* **74**, 2128–2137.
- Majlessi, L., Prados-Rosales, R., Casadevall, A., and Brosch, R. (2015). Release of mycobacterial antigens. *Immunol. Rev.* **264**, 25–45.
- Marrichi, M., Camacho, L., Russell, D.G., and DeLisa, M.P. (2008). Genetic toggling of alkaline phosphatase folding reveals signal peptides for all major modes of transport across the inner membrane of bacteria. *J. Biol. Chem.* **283**, 35223–35235.
- Pym, A.S., Brodin, P., Brosch, R., Huerre, M., and Cole, S.T. (2002). Loss of RD1 contributed to the attenuation of the live tuberculosis vaccines *Mycobacterium bovis* BCG and *Mycobacterium microti*. *Mol. Microbiol.* **46**, 709–717.

- Pym, A.S., Brodin, P., Majlessi, L., Brosch, R., Demangel, C., Williams, A., Griffiths, K.E., Marchal, G., Leclerc, C., and Cole, S.T. (2003). Recombinant BCG exporting ESAT-6 confers enhanced protection against tuberculosis. *Nat. Med.* **9**, 533–539.
- Queval, C.J., Song, O.R., Carralot, J.P., Saliou, J.M., Bongiovanni, A., Deloison, G., Deboosère, N., Jouny, S., Iantomasi, R., Delorme, V., et al. (2017). *Mycobacterium tuberculosis* controls phagosomal acidification by targeting CISH-mediated signaling. *Cell Rep.* **20**, 3188–3198.
- Ramakrishnan, P., Aagesen, A.M., McKinney, J.D., and Tischler, A.D. (2015). *Mycobacterium tuberculosis* resists stress by regulating PE19 expression. *Infect. Immun.* **84**, 735–746.
- Rogerson, B.J., Jung, Y.J., LaCourse, R., Ryan, L., Enright, N., and North, R.J. (2006). Expression levels of *Mycobacterium tuberculosis* antigen-encoding genes versus production levels of antigen-specific T cells during stationary level lung infection in mice. *Immunology* **118**, 195–201.
- Sayes, F., Sun, L., Di Luca, M., Simeone, R., Degaiffier, N., Fiette, L., Esin, S., Brosch, R., Bottai, D., Leclerc, C., and Majlessi, L. (2012). Strong immunogenicity and cross-reactivity of *Mycobacterium tuberculosis* ESX-5 type VII secretion: encoded PE-PPE proteins predicts vaccine potential. *Cell Host Microbe* **11**, 352–363.
- Sayes, F., Pawlik, A., Frigui, W., Gröschel, M.I., Crommelynck, S., Fayolle, C., Cia, F., Bancroft, G.J., Bottai, D., Leclerc, C., et al. (2016). CD4+ T cells recognizing PE/PPE antigens directly or via cross reactivity are protective against pulmonary *Mycobacterium tuberculosis* infection. *PLoS Pathog.* **12**, e1005770.
- Shi, L., North, R., and Gennaro, M.L. (2004). Effect of growth state on transcription levels of genes encoding major secreted antigens of *Mycobacterium tuberculosis* in the mouse lung. *Infect. Immun.* **72**, 2420–2424.
- Simeone, R., Majlessi, L., Enninga, J., and Brosch, R. (2016). Perspectives on mycobacterial vacuole-to-cytosol translocation: the importance of cytosolic access. *Cell. Microbiol.* **18**, 1070–1077.
- Solans, L., Gonzalo-Asensio, J., Sala, C., Benjak, A., Uplekar, S., Rougemont, J., Guilhot, C., Malaga, W., Martin, C., and Cole, S.T. (2014). The PhoP-dependent ncRNA Mcr7 modulates the TAT secretion system in *Mycobacterium tuberculosis*. *PLoS Pathog.* **10**, e1004183.
- Stanley, S.A., and Cox, J.S. (2013). Host-pathogen interactions during *Mycobacterium tuberculosis* infections. *Curr. Top. Microbiol. Immunol.* **374**, 211–241.
- Van Regenmortel, M.H. (2009). What is a B-cell epitope? *Methods Mol. Biol.* **524**, 3–20.
- Vordermeier, H.M., Hewinson, R.G., Wilkinson, R.J., Wilkinson, K.A., Gideon, H.P., Young, D.B., and Sampson, S.L. (2012). Conserved immune recognition hierarchy of mycobacterial PE/PPE proteins during infection in natural hosts. *PLoS ONE* **7**, e40890.